Research on Chemical Intermediates
https://doi.org/10.1007/s11164-019-03822-3

Preparation of Co-Pd bimetallic nanoparticles encapsulated in bamboo-like N-doped mesoporous carbon by a facile one-pot method for green Suzuki coupling

Li Wu[1,2,3] · Yu Long[3] · Jiantai Ma[3] · Gongxuan Lu[1]

Received: 19 March 2019 / Accepted: 3 April 2019

Abstract

CoPd bimetallic nanoparticles (NPs) were successfully encapsulated in bamboo-like N-doped mesoporous carbon (bNMC) via a facile one-pot method through combination of dissolving chelation and carbonization reactions. The morphology, structure and composition of CoPd-bNMC was verified by detailed characterization including SEM, TEM, EDX, XPS, XRD, N_2 adsorption–desorption, VSM, and ICP. The as-prepared CoPd/bNMC showed excellent activity and selectivity for Suzuki coupling under mild and green condition. Though the Pd content of CoPd/bNMC was half of Pd/bNMC, the catalytic performance of CoPd/bNMC was almost the same with Pd/bNMC, which was caused by its special bimetallic alloy structure, high BET surface area and pore volume. Importantly, CoPd/bNMC with magnetic property can be separated using external magnetic field and reused for five consecutive runs in the reaction of Suzuki crossing without significant loss of activity. It was found the Pd content only showed slight loss (2.3 wt.%) after five reused reactions, which was because CoPd bimetallic NPs were inside the bamboo-like N-doped mesoporous carbon.

Keywords Co-Pd · Bimetallic nanoparticles · N-doped mesoporous carbon · Suzuki coupling

✉ Jiantai Ma
majiantai@lzu.edu.cn

✉ Gongxuan Lu
gxlu@lzb.ac.cn

[1] Lanzhou Institute of Chemical Physics, CAS, Lanzhou 730000, People's Republic of China

[2] University of Chinese Academy of Sciences, Beijing 100049, People's Republic of China

[3] College of Chemistry and Chemical Engineering, Lanzhou University, Lanzhou 730000, People's Republic of China

Published online: 22 April 2019

Introduction

Noble-metal-based heterogeneous catalysts have been widely applied for selective hydrogenation [1–8], oxidation [9–16], carbon–carbon coupling reactions [17–19] and electrocatalysis [20–23]. Although noble-metal catalysts are acknowledged to be fine option due to superior catalytic properties, the simple noble metal NPs are prone to merge and agglomerate because of their high surface energy and high reactivity. Moreover, they are expensive, low atomic utilization rate and easy to lose, poisoning their autologous activity greatly, which is a major limitation of their practical applications. Many strategies have been developed to improve stability and reduce cost of noble metal catalysts [24–31]. As an effective method, transition metals, such as Fe, Co, Ni were introduced to prepare noble-metal–M (M=Fe, Co, Ni) bimetallic alloy catalyst. Noble-metal-M alloy catalyst can not only reduce the loading dosage of noble-metal, but also can be beneficial for increase catalytic efficiency and selectivity [32–35]. For this kind of alloy catalysts containing noble and non-noble metals, it is crucial to optimize the interaction and proportion of noble and non-noble metals [36]. In order to achieve high catalytic activity and selectivity, Co-based bimetallic alloy catalysts have attracted extensive attention [37–44].

To avoid nanocatalyst losses in separation processes or diffusion factors, carbon nanotubes are a better choice than conventional carriers [45, 46]. Metal NPs loaded in carbon nanotubes or inside carriers can greatly inhibit metal loss. Thereinto, N-doped mesoporous carbon materials have been identified as the most promising catalyst supports for the development of robust and efficient catalytic systems, due to its unique chemical, electrical and functional properties [47–51]. It is widely accepted that N-doping can enhance the interaction between metal and support and provide high electron mobility, thus greatly improving its catalytic performance and stability [52, 53]. In addition, the unique porosity and nanostructure of N-doped mesoporous carbon coated metal catalyst endowed the catalysts other advantages, such as high shape-selectivity for various heterogeneous catalytic reaction. Therefore, N-doped mesoporous carbon coated bimetallic alloy catalyst may effectively increase both catalytic efficiency and selectivity, as well as improve stability.

Nowadays, many efforts have been devoted to design a simple and effective method to easily prepare N-doped mesoporous carbon coated metal catalyst. As well known, one-pot synthetic process is the ideal method for preparing multicomponent catalyst. Herein, we report a facile, efficient and large-scale approach to prepare N-doped mesoporous carbon coated CoPd bimetallic alloy catalysts. A simple one-pot preparation method was used to prepare bimetallic cobalt palladium NPs/bamboo-like N-doped mesoporous carbon (CoPd/bNMC) composite by combination of dissolving chelation and carbonization reactions. The as-prepared CoPd/bNMC composite was applied for the Suzuki coupling reaction and showed excellent activity and selectivity for Suzuki coupling under mild and green condition.

Experimental

Materials

$Co(NO_3)_2{\cdot}6H_2O$, $Pd(Ac)_2$, $NaBH_4$, methanol, Melamine (MA), polyacrylonitrile (PA) and were purchased from Kelong Chemical Reagents Company (Chengdu, China). *N*, *N*-dimethylformamide (DMF) and ethanol were obtained from Sinopharm Chemical Reagent Co. Ltd. (China). All chemicals used in this study were of analytical grade and used without further purification.

Synthesis of the CoPd/bNMC catalysts

The CoPd/bMNC catalyst was prepared via one-pot pyrolysis of a homogeneous mixture of $Co(NO_3)_2{\cdot}6H_2O$, $Pd(Ac)_2$, PA, and MA at high temperature ($\geq$ 700 °C) under a N_2 atmosphere. In a typical synthesis procedure: 1.06 g of PA and 500 mg of $Co(NO_3)_2{\cdot}6H_2O$ were first dissolved in 100 mL of DMF in a 250-mL round-bottom flask-2-neck and stirred for 1 h at 100 °C (oil bath), until a homogeneous solution was formed. Second, 20 g of melamine were slowly added to the as-prepared homogeneous solution followed by mechanical stirring for 2 h to obtain a thick slurry, and corresponding molar quantity palladium acetate were added to the flask and stirred for 1 h at room temperature, which was evaporated on a rotary evaporator and ground into powder. The as-obtained powder was subsequently pyrolysis at 800 °C for 1 h via programmed heating at 10 °C/min under N_2 atmosphere, to obtain the CoPd/bMNC nanocatalyst. In addition, a Co-free material (bMNC) and Pd-free material (bMNC) were prepared by a similar one-pot pyrolysis method without adding $Co(NO_3)_2{\cdot}6H_2O$ or $Pd(Ac)_2$.

CoPd/bMNC catalyst for Suzuki reaction

A mixture of aryl halide (1 mmol), arylboronic acid (1.5 mmol), PdCo/bNMC (for aryl bromide 1 mol %, for aryl chloride 2 mol %), and K_2CO_3 (2 mmol) was stirred in EtOH-H_2O at suitable temperature for indicated time in air. After completion of the reaction, the mixture was cooled to room temperature, separated by magnetic decantation, and extracted by Et_2O (10 mL) for three times. And then the organic phase was combined and evaporated under reduced pressure. Finally, the reaction yields were obtained by GC. the concrete calculation method of the yields is gas chromatography area normalization method.

Characterizations

Transmission electron microscopy (TEM, FEI Tecnai G2 F30,200 kV) was used to observe the morphology and elemental mapping of the prepared catalysts. Powder X-ray diffraction (PXRD, Rigaku D/max-2400) was performed in the 2θ range of 10–90 degree using Cu-Ka radiation ($k = 1.542$ Å) as the X-ray source operating at 50 kV and 300 mA. X-ray photoelectron spectroscopy (XPS, Perkin-Elmer

PHI-5702) was employed to analyze the surface electronic states of the prepared catalysts. Brunauer–Emmett–Teller (BET, Micromeritics ASAP 2010) measurements were employed to measure the pore size distribution, surface area and the pore volume. Inductively coupled plasma atomic emission spectroscopy (ICP-AES) was employed to analyze the Co and Pd content in the obtained CoPd/bMCN samples. The magnetic properties of the prepared catalysts were measured by a vibrating sample magnetometer (VSM) at room temperature by varying the applied magnetic field from 0 to 20 kOe. GC–MS (Agilent 5977E) was employed for monitoring the reaction conversion and selectivity. Agilent Technologies 7820 A is used for analysis, the column length is 30 m and the diameter is 0.250 nm.

The general preparation strategy of CoPd/bMCN is displayed in Scheme 1.

Results and discussion

Characterization of catalysts

The nanotube mesoporous structure CoPd/bMNC samples were prepared by pyrolysis a mixture of melamine, $Co(NO_3)_2{\cdot}6H_2O$ and PA, and Scheme 1 displays the simple synthetic pathway of the CoPd/bMNC. In this experiment, melamine acts as not only a carbon source, but a nitrogen source, which chelates positively charged melamine and cobalt ions, thus forming a homogeneous chelate precipitate in aqueous solution by the protonated carboxyl group. Meanwhile, melamine can be easy to decompose when the temperature beyond 200 °C, and form layered graphitic carbon nitride when the temperature is 550 °C through a slow heating rate. Moreover, when the temperature is up to 600 °C, the layered graphitic carbon nitride will decompose immediately. In the pyrolysis process, carbonized polyacrylonitrile (PA) is condensed to the carbon skeleton. Because of forming better porous materials, the calcination temperature setup of catalysts is 800 °C.

Figure 1 shows SEM image of and TEM images of CoPd/bMCN nanocatalyst. As shown in Fig. 1a, SEM image of as-prepared CoPd/bMCN was tubular structures similar to carbon nanotubes. From the TEM image in Fig. 1b, it could be easily observed CoPd/bMCN was bamboo-like nanotubes structure. And the CoPd bimetallic NPs were encapsulated in bMCN. As evidenced in Fig. 1c, the average diameters of CoPd NPs were approximately 8 and 6 nm. The high-angle

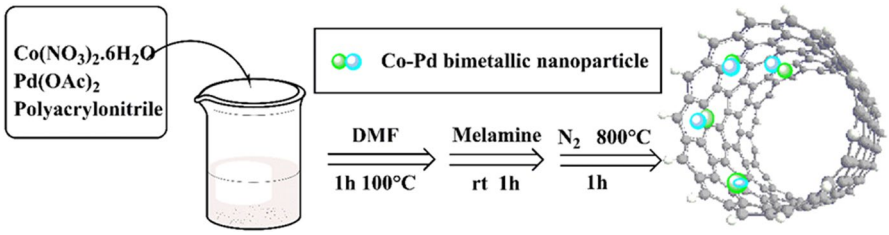

Scheme 1 Total synthetic strategy for the CoPd/bMCN catalysts

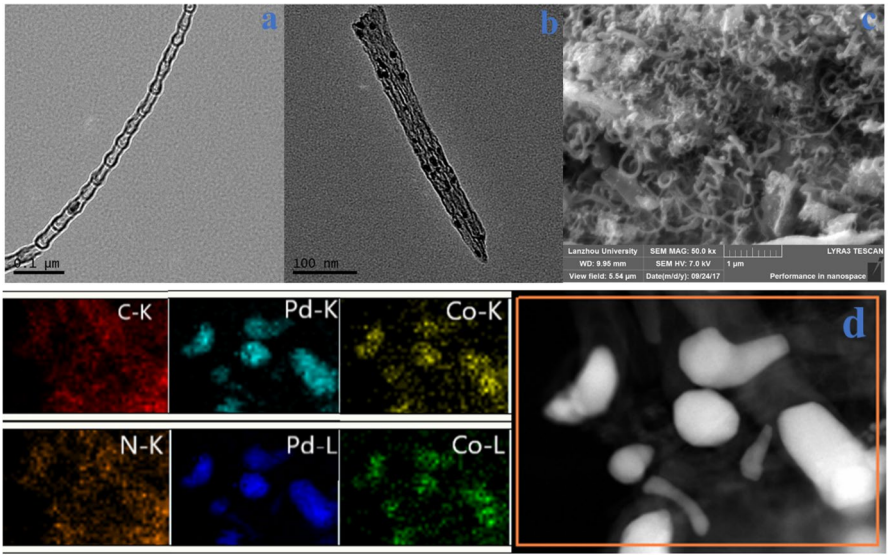

Fig. 1 **a**, **b** The TEM images of CoPd/bMNC, **c** The SEM images of CoPd/bMNC, **d** EDX mapping of CoPd/bMNC

annular dark-field scanning transmission electron microscopy (HAADF-STEM) was also applied to examine the component and structure of CoPd/bMCN, which are displayed in Fig. 1d. From the results of HAADF-STEM, we can easily find out CoPd NPs show good dispersion, and the doped N was successfully inserted into carbon material. Element distribution mappings of selected area revealed the really existence of CoPd bimetallic NPs encapsulated in bMCN.

The chemical compositions of the as-prepared CoPd/bMCN catalyst were measured by XPS measurements. The wide-range XPS spectrum of CoPd/bMNC (shown in Fig. 2a) demonstrates the presence of elemental C, N, O, Co and Pd in the as –prepared CoPd/bMNC sample. To further explore the valence state of Co and Pd, the Pd 3d and Co 2p XPS spectra of the sample were also acquired. The peak at around 780 eV is assigned to the Co^0 (shown in Fig. 2b), indicating the appearance of cobalt nanoparticles in the pyrolysis process, and the peak at around 787 eV is attributed to the cobalt oxide, which may be caused by the oxidization of cobalt nanoparticles in the XPS sampling process. From these results we can conclude that the Co–O was indeed formed, followed by the replacement of N by O in CoNx, and finally Co^0 was formed through the decomposition of CoNx or reduction with carbon at high-temperature under inert atmosphere. In the Pd 3d XPS spectrum (Fig. 2c), two characteristic peaks attributed to Pd $3d_{3/2}$ and Pd $3d_{5/2}$ at around 338.7 and 333.5 eV indicate that the existence of Pd nanoparticles in the CoPd/bMCN catalyst. In addition, the chemical compositions of different elementals of the as-prepared samples are exhibited in Table 1, and the Co and N contents the CoPd/bMCN catalyst are 11.95 and 14.1 wt.%, respectively.

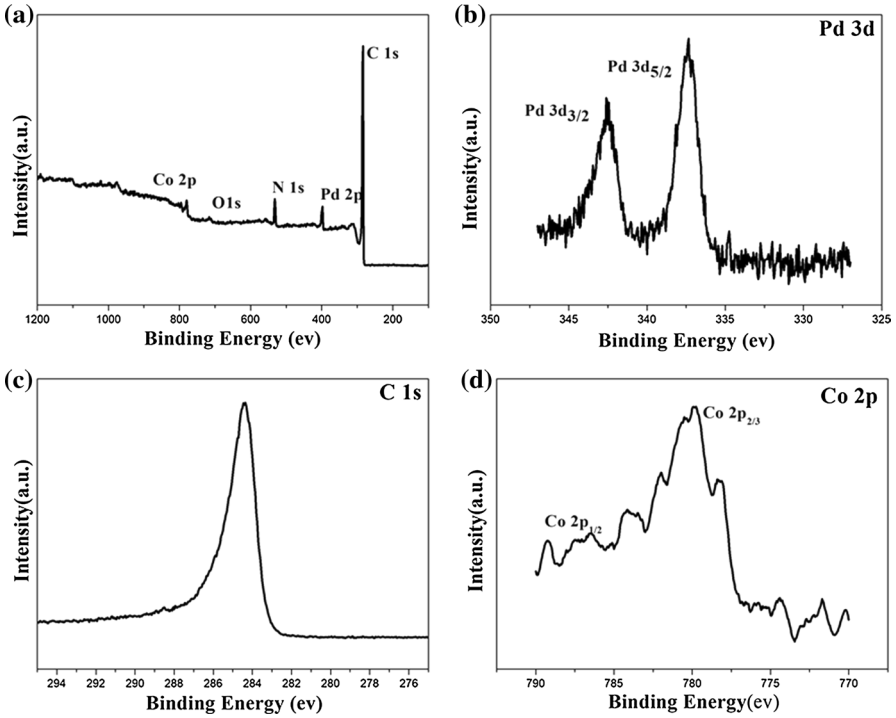

Fig. 2 **a** the wide-range XPS spectrum of CoPd/bMNC; **b** the Pd 3d and **c** C1s **d** Co 2p region of CoPd/bMNC

Table 1 Texture parameters and the element content of the prepared catalysts

Catalyst	Surface area ($m^2\ g^{-1}$)	Pore size (nm)	Pore volume ($cm^3\ g^{-1}$)	Pd (wt.%)	Co (wt.%)	N (wt.%)
Co/bMCN	251.89	6.56	0.41	0	3.98	15.90
Pd/bMNC	269.96	4.47	0.41	3.05	0	14.80
CoPd/bMCN	281.69	3.75	0.26	1.72	2.95	14.10

XRD analysis was used to examine the structures of Co/bMNC, Pd/bMNC and CoPd/bMNC samples, the results are displayed in Fig. 3. The peak at around 25° is assigned to the carbon (002) plane of CNT diffraction of amorphous carbon. For the XRD pattern of CoPd/bMNC, the peaks at 40°, 46°, 68°, and 83° are attributed to the Pd (111), (200), (220) and (311) crystal planes respectively (JCPDS NO.05-0681), for bimetallic NPs, the Pd species also show strong diffraction peaks, further demonstrating that the Pd species of CoPd/bMNC show a face-centered cubic structure phase, corresponding to the standard Pd card (JCPDS NO.05-0681). Moreover, the diffraction peaks attributed to Pd in CoPd/bMNC shift slightly to higher 2θ values compared with the standard Pd card (JCPDS NO.05-0681), proving the lattice contraction caused by the incorporation

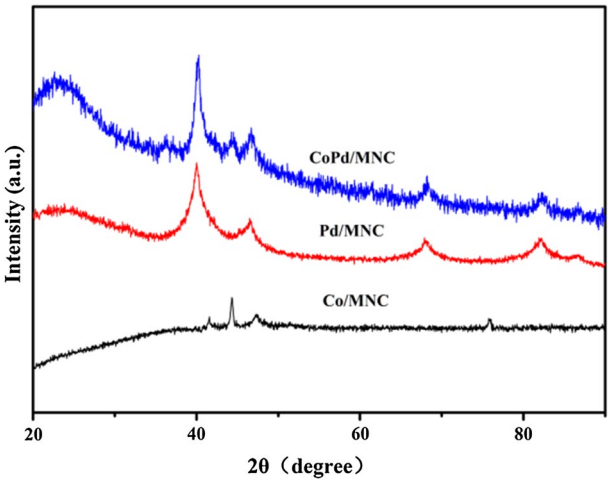

Fig. 3 XRD patterns of the prepared catalysts **a** CoPd/bMNC, **b** Co/bMNC, and **c** Co/bMNC

of Co species into the Pd face-centered cubic structure. This is an evidence of Pd-Co alloy formation.

The N_2 adsorption–desorption profiles and pore size distribution for Co/bMNC, Pd/bMNC and CoPd/bMNC catalysts are displayed in Fig. 4. According to the IUPAC classification, the isotherms with a large hysteresis loop in the relative pressure (P/P_0) range of 0.4–1.0 show a type IV curve, corresponding to the characteristics of mesoporous materials with micro- and mesoporous pore size distribution. The large hysteresis loop suggests that a capillary condensation phenomenon has occurred in the mesoporous structure. However, Pd/bMCN has a very small hysteresis loop, which should be due to the formation of dense graphitic carbon nitride. CoPd/bMNC shows a higher specific surface area, originating from the

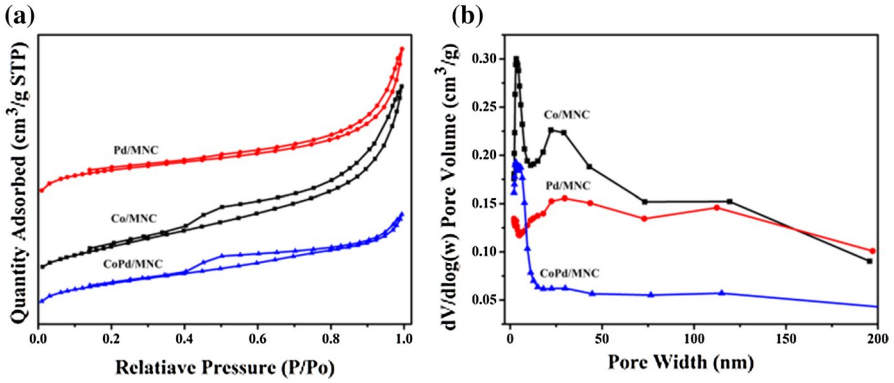

Fig. 4 **a** Nitrogen adsorption–desorption isotherm plots of the prepared CoPd/bMCN materials that carbonized at different temperatures. **b** Pore size distributions of the prepared CoPd/bMCN materials

porous and multi-channel bamboo-like structure in the rod solids as evidenced in Fig. 2. Table 1 summarizes the BET surface area, pore volume, and average pore size of the prepared catalysts (i.e., Co/bMCN, CoPd/bMCN, Pd/bMCN). As shown in Table 1, CoPd/bMCN exhibited the highest BET surface area and pore volume (281.69 $m^2\ g^{-1}$, and 0.26 $cm^3\ g^{-1}$ respectively), with an average pore size of 3.7 nm. The more developed mesoporous of those materials pyrolyzed at high temperatures was thought to enhance the exposure of the Co active sites, thereby increasing its catalytic activity. The elemental compositions of the prepared catalysts are also demonstrated in Table 1, the CoPd/bMCN catalyst showed N and Co contents of 14.1 and 2.95 wt.%, respectively.

The magnetic property of CoPd/bMCN was also tested (displayed in Fig. 5). According ro the magnetic measurement, the magnetization saturation value of CoPd/bMCN is 9.55 emu g^{-1}. Owing to its magnetite content, CoPd/bMCN could be rapidly separated from the reaction mixture with the external magnetic field. This characteristic property can provide a more portable and efficient way to separate the CoPd/bMCN catalyst from the after reaction system for recycle under the external magnetic field.

Catalytic activity, generality and recyclability for Suzuki coupling reaction by CoPd/bMNC

We have chosen Suzuki coupling reaction as the model reaction, the optimal reaction conditions, the catalysts composition, the general applicability, and recyclability of CoPd/bMNC were investigated.

The optimized reaction condition for Suzuki coupling reaction by CoPd/bMNC was examined (Table 2). All reactions were tested under N_2 atmosphere. As shown in Table 2, entries 1-5, under the reaction conditions of 0.5 mmol of iodobenzene, 0.75 mmol of phenylboronic acid, 5.0 mol % of CoPd/MNC catalyst and 2.0 mmol

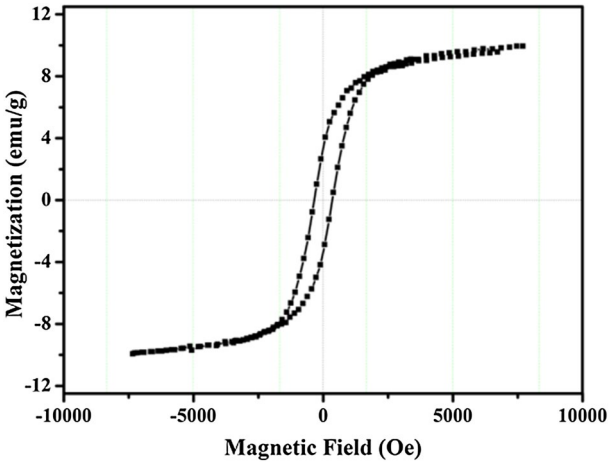

Fig. 5 Room-temperature magnetization curves of the CoPd/bMCN catalyst

Table 2 Optimization of conditions for the Suzuki reaction of iodobenzene with phenylboronic acid

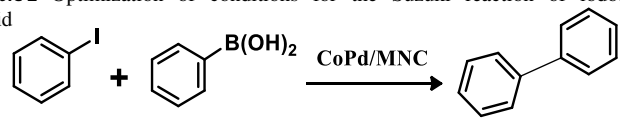

Entry	Solvent	Catalyst	Base	Time (h)	Yield (%)[a]
1	DMF	CoPd/bMNC	K_2CO_3	0.5	60.6
2	Toluene	CoPd/bMNC	K_2CO_3	0.5	43.3
3	H_2O	CoPd/bMNC	K_2CO_3	0.5	68.2
4	EtOH	CoPd/bMNC	K_2CO_3	0.5	97.9
5	EtOH-H_2O	CoPd/MNC	K_2CO_3	0.5	95.8
6	EtOH-H_2O	CoPd/bMNC	$NaHCO_3$	0.5	78.1
7	EtOH-H_2O	CoPd/MNC	NaOAc	0.5	11.4
8	EtOH-H_2O	CoPd/bMNC	KOH	0.5	45.1
9	EtOH-H_2O	CoPd/bMNC	No base	0.5	Trace
10	EtOH-H_2O	Pd/bMNC	K_2CO_3	0.5	97.5
11	EtOH-H_2O	Co/bMNC	K_2CO_3	0.5	8.3

Reaction conditions: iodobenzene (0.5 mmol), phenylboronic acid (0.75 mmol), H_2O (2.5 mL), EtOH (2.5 mL), CoPd/MNC (5.0 mol %), 80 °C

[a]Determined by using GC

base at 80 °C in a 5 mL solvent, the solvent effect on this reaction was firstly studied, the screening of many solvents exhibites that EtOH/H_2O is the most suitable solvent. Further, different bases were investigated on this Suzuki coupling reaction, because different bases have different influences on catalytic performance. As shown in Table 2, entries 6-9, we can know that the reaction gave no product in the absence of base, and K_2CO_3 showed the best catalytic performance in various bases. Under the optimal reaction condition, the catalytic activities of Co/bMNC and Pd/bMNC for the Suzuki C–C coupling reaction were tested (Table 2, entries 10, 11). It is found Co/bMNC exhibited a very low catalytic performance for this Suzuki C–C coupling reaction (8.3% yield), while, Pd/bMNC showed a high yield of target product. Though the catalytic performance of Pd/bNMC (97.5% yield) was a little higher than CoPd/bNMC (95.8% yield), the Pd content of Pd/bNMC was more than twice the Pd content of CoPd/bNMC, which was caused by its special bimetallic structure. Notably, the Mott-Schottky-based CoPd/bMNC heterogeneous catalyst can greatly enhance the catalytic activity through designing the Mott-Schottky interface in metal (CoPd) and bMNC. Besides, introducing cobalt to form the bimetallic alloy catalytic system can effectively prevent the noble nanoparticles agglomeration as well activating the Pd center through electron charge transfer between Pd and Co.

The generality of this Suzuki coupling reaction was also studied, different substituted phenylboronic acid with different halides (I, Br, Cl) were tested under the optimized conditions. CoPd/bMNC showed high yield of targat products when reacting phenyl iodides, bromides and chlorides with phenylboronic acid (Table 3, entries 1–9). Aryl halides could bear both electron-withdrawing

Table 3 Heterogeneous Suzuki–Miyaura reaction of aryl halides ($R_1C_6H_4X$) with phenylboronic acid ($R_2C_6H_4B(OH)_2$) catalysed by CoPd/MNC[a]

Entry	R_1	X	R_2	Time (h)	Yield (%)[b]
1	H	I	H	0.5	99.9
2	H	I	CH_3	1	90.2
3	4-CH_3	I	CH_3	2 h	88.9
4	4-$COCH_3$	I	H	2 h	91.5
5	4-CH_3	I	H	2 h	93.2
6	4-OH	I	H	2 h	94.8
7	4-NO_2	I	H	2 h	93.1
8	4-OH	I	Cl	2 h	73.0
9	4-NO_2	I	Cl	2 h	71.3
10	4-OCH_3	Br	Cl	2 h	83.6
11	H	Br	H	2 h	89.7
12	H	Cl	H	2 h	23.9

[a]Reaction conditions: iodobenzene (0.5 mmol), phenylboronic acid (0.75 mmol), H_2O (2.5 mL), EtOH (2.5 mL), CoPd/MNC (5.0 mol%)

[b]Determined by using GC. Our chromatographic model is Agilent Technologies 7820A, the column length is 30 m and the diameter is 0.250 nm, the TIC image integral used to compute the percentage

and electron-releasing groups reacting with phenylboronic acid to acquire high yield of products. It is noteworthy that 2-bromothiophene and 2-iodothiophene reacting with phenylboronic acid give 99.9 and 94.8% product yields, respectively (shown in Table 3, entries 1 and 6).

In view of both industrial production and green chemistry, the recyclability of the catalyst is also an important index to evaluate the comprehensive performance of catalyst. So the recyclability of CoPd/bMNC was estimated. In this recycle experiment, the CoPd/bMNC catalyst was separpted from reaction mixture by using a magnet after each cycle run, and and exhaustively washed with deionized water and ethanol. Finally, the catalyst was dried at 80 °C for 24 h and reused for the next cycle reaction experiment. It can be seen that the CoPd/bMNC catalyst could be applied for five times and still maintain high production yields (Fig. 6). The good catalytic perfomance could be due to the strong catalysis synergistic effect of Co nanoparticles and Pd nanoparticles with active sites of N-doped carbon materials. Moreover, the morphology and structure of the reused catalyst was also investgated. As shown in Fig. 6, the TEM image of the reused CoPd/bMNC indicates that the catalyst shows no change in morphology after five times reaction. The contents of Pd of CoPd/bMNC before and after five times reaction were also measured by applying ICP-AES analysis, which is 2.65 and 2.59 wt.% respectively. This result indicates that Palladium is stably supported on the BMNC and there is almost no leaching during the reaction.

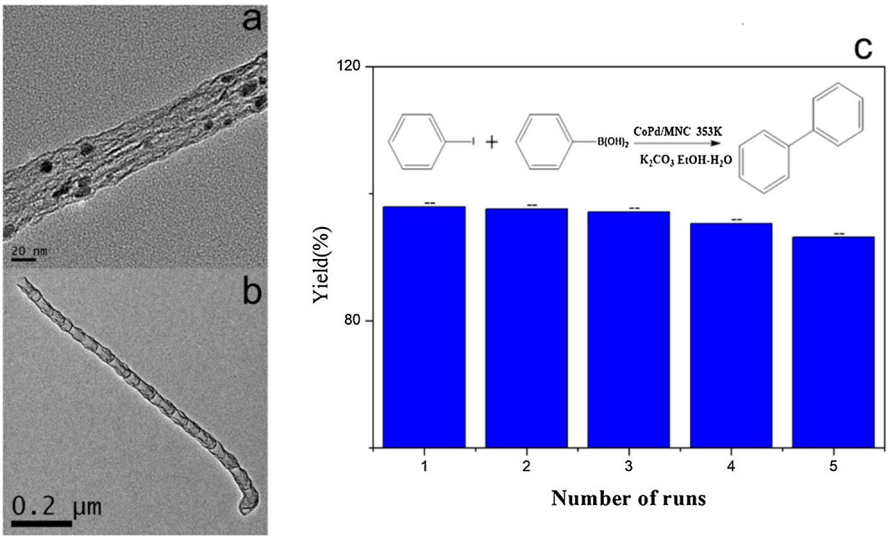

Fig. 6 **a**, **b** The TEM images of CoPd/MNC after five runs. **c** Recycle of the CoPd/MCN catalyst

Conclusions

In summary, we synthesized highly active bimetallic CoPd/bMNC nanoparticle catalysts, and showed good activity towards Suzuki coupling reaction in water–ethanol solution for various substrates. Though the Pd content of CoPd/bNMC was half of Pd/bNMC, the catalytic performance of CoPd/bNMC was almost the same with Pd/bNMC. Notably, the Mott-Schottky-based CoPd/bMNC heterogeneous catalyst can greatly enhance the catalytic activity through designing the Mott-Schottky interface in metal (CoPd) and bMNC. Besides, introducing cobalt to form the bimetallic alloy catalytic system can effectively prevent the noble nanoparticles agglomeration as well activating the Pd center through electron charge transfer between Pd and Co. Moreover, the CoPd/bMNC catalyst has the advantages of low-price, easy to recycle from the reaction mixture through the magnetic field and the CoPd/bMNC catalyst can be prepared in large-scale, we think our catalyst could be applied more widely in various fields. Overall, such a low-cost and high-performance nanocatalyst may bring new design opportunities for C–C coupling catalysis on an industrial scale in the future.

Acknowledgements This research was supported by the National Natural Science Foundation of China (China, 21433007, 21872066).

References

1. F. Meemken, A. Baiker, Chem. Rev. **117**, 11522 (2017)

2. Y. Long, Y. Liu, Z. Zhao, S. Luo, W. Wu, L. Wu, H. Wen, R.-Q. Wang, J. Ma, J. Colloid Interf. Sci. **496**, 465 (2017)
3. H.N. Chai, B. Liu, A.Q. Liu, K. Yu, J. Mol. Catal. (China) **32**, 481 (2018)
4. H. Cao, X. Chen, Y. Du, C.H. Liang, J. Mol. Catal. (China) **32**, 501 (2018)
5. G.X. Li, Q. Li, X.L. Zeng, J. Bian, H.W. Li, H.F. Mu, J. Mol. Catal. (China) **31**, 316 (2017)
6. L.G. Chen, X.H. Zhang, Q.Y. Liu, Q. Zhang, T.J. Wang, C.G. Wang, L.L. Ma, J. Mol. Catal. (China) **31**, 267 (2017)
7. Y. Long, B. Yuan, J. Niu, X. Tong, J. Ma, New J. Chem. **39**, 1179 (2015)
8. C. Huang, X. Wang, F. Yu, B. Yuan, C. Xie, S. Yu, Res. Chem. Intermed. **44**, 13 (2018)
9. Y. Long, Z. Zhao, L. Wu, S. Luo, H. Wen, W. Wu, H. Zhang, J. Ma, Mol. Catal. **433**, 291 (2017)
10. J.H. Guo, C.X. Lin, C.J. Jiang, P.Y. Zhang, Appl. Surf. Sci. **475**, 237 (2019)
11. Q. Zhang, Q. Liu, P. Ning, X. Liu, L. Xu, Z. Song, Y. Duan, T. Zhang, Res. Chem. Intermed. **43**, 2017 (2017)
12. L.L. Chen, Z.X. Wang, B.X. Dou, K. Han, J. Y. Xin **32**, 574 (2018)
13. H.X. Guo, R.X. Yan, X.H. Xi, J. Mol. Catal. (China) **32**, 471 (2018)
14. S.C. Chen, F. Han, J.H. Liu, C.G. Xia, J.X. Ma, J. Mol. Catal. (China) **32**, 382 (2018)
15. H.P. Yan, Y.C. Zhang, H.Y. Zhang, J.Q. Zhao, J Mol Catal (China) **32**, 117 (2018)
16. L. Liu, C.H. Zheng, X. Gao, J. Mol. Catal. (China) **32**, 54 (2018)
17. J. Xia, Y. Fu, G. He, X. Sun, X. Wang, Appl. Catal. B.-Environ. **200**, 39 (2017)
18. Y. Long, K. Liang, J. Niu, X. Tong, B. Yuan, J. Ma, New J. Chem. **39**, 2988 (2015)
19. M.M. Khodaei, A. Alizadeh, M. Haghipour, Res. Chem. Intermed. (2019)
20. J. Wang, F. Xu, H.Y. Jin, Y.Q. Chen, Y. Wang, Adv. Mater. **29**, 35 (2017)
21. S. Gao, M.X. Yang, S.M. Li, J. Mei, S. Xie, H. Liu, J. Mol. Catal. (China) **32**, 261 (2018)
22. Z.K. Xie, X.Y. Chen, W.B. Hu, X.G. Shu, X.H. Zhou, W.W. Chen, J. Mol. Catal. (China) **32**, 520 (2018)
23. Y. Ren, D.R. Liu, Y. Pan, J. Feng, W. Xiong, D.H. Qiu, J. Mol. Catal. (China) **32**, 8 (2018)
24. J. Tang, R.R. Salunkhe, J. Liu, N.L. Torad, M. Imura, S. Furukawa, Y. Yamauchi, J. Am. Chem. Soc. **137**, 1572 (2015)
25. K. Shen, X. Chen, J. Chen, Y. Li, ACS Catal. **6**, 5887 (2016)
26. W. Xia, R. Zou, L. An, D. Xia, S. Guo, Energy Environ. Sci. **8**, 568 (2015)
27. X. Li, Y. Fang, X. Lin, M. Tian, X. An, Y. Fu, R. Li, J. Jin, J. Ma, J. Mater. Chem. A. **3**, 17392 (2015)
28. A. Aijaz, Q. Xu, J. Phys. Chem. Lett. **5**, 1400 (2014)
29. C. Bai, X. Yao, Y. Li, ACS Catal. **5**, 884 (2015)
30. R.V. Jagadeesh, A.-E. Surkus, H. Junge, M.-M. Pohl, J. Radnik, J. Rabeah, H. Huan, V. Schünemann, A. Brückner, M. Beller, Science **342**, 1073 (2013)
31. Z. Wei, J. Wang, S. Mao, D. Su, H. Jin, Y. Wang, F. Xu, H. Li, Y. Wang, ACS Catal. **5**, 4783 (2015)
32. Z.P. Dong, X.D. Le, C.X. Dong, W. Zhang, X.L. Li, J.T. Ma, Appl. Catal. B-Environ. **162**, 372 (2015)
33. J. Yang, W.D. Wang, Z.P. Dong, J. Colloid Interface Sci. **524**, 84 (2018)
34. X.L. Cui, Y. Long, X. Zhou, G.Q. Yu, J. Yang, M. Yuan, J.T. Ma, Z.P. Dong, Green Chem. **20**, 1121 (2018)
35. S. Komeili, M.T. Ravanchi, A. Taeb, Res. Chem. Intermed. **44**, 1335 (2018)
36. H. Fang, J.H. Yang, M. Wen, Q.S. Wu, Adv. Mater. **30**, 10 (2018)
37. H. Ma, H. Wang, T. Wu, C. Na, Appl. Catal. B-Environ. **180**, 471 (2016)
38. R.V. Jagadeesh, D. Banerjee, P.B. Arockiam, H. Junge, K. Junge, M.-M. Pohl, J. Radnik, A. Brückner, M. Beller, Green Chem. **17**, 898 (2015)
39. P. Hu, M. Long, Appl. Catal. B-Environ. **181**, 103 (2016)
40. R.V. Jagadeesh, K. Murugesan, A.S. Alshammari, H. Neumann, M.-M. Pohl, J. Radnik, M. Beller, Science **358**, 326 (2017)
41. X.L. Cui, H. Li, G.Q. Yu, M. Yuan, J. Yang, D. Xu, Y.M. Hou, Z.P. Dong, Int. J. Hydrogen Energy **42**, 27055 (2017)
42. P. Zhou, Z. Zhang, L. Jiang, C. Yu, K. Lv, J. Sun, S. Wang, Appl. Catal. B-Environ. **210**, 522 (2017)
43. X. Cui, K. Liang, M. Tian, Y. Zhu, J. Ma, Z. Dong, J. Colloids Interface Sci. **501**, 231 (2017)
44. T.A. Revathy, T. Sivaranjani, A.A. Boopathi, S. Sampath, V. Narayanan, A. Stephen, Res. Chem. Intermed. **45**, 815 (2019)
45. Y.B. Yan, J.W. Miao, Z.H. Yang, F.X. Xiao, H.B. Yang, B. Liu, Y.H. Yang, Chem. Soc. Rev. **44**, 3295 (2015)

46. B.T. Liu, Y.L. Xu, S.Y. Zhang, X.M. Lv, Y.Q. Ling, Z.J. Zhou, J. Liu, Mater. Lett. **239**, 124 (2019)
47. B. Chen, L. Wang, W. Dai, S. Shang, Y. Lv, S. Gao, ACS Catal. **5**, 2788 (2015)
48. A. Aijaz, J. Masa, C. Rösler, W. Xia, P. Weide, A.J.R. Botz, R.A. Fischer, W. Schuhmann, M. Muhler, Angew. Chem. Int. Ed. **55**, 4087 (2016)
49. J. Wei, Y. Hu, Y. Liang, B. Kong, J. Zhang, J. Song, Q. Bao, G.P. Simon, S.P. Jiang, H. Wang, Adv. Funct. Mater. **25**, 5768 (2015)
50. M.Y. Fan, Y. Long, Y.Y. Zhu, X.W. Hu, Z.P. Dong, Appl. Catal. a-Gen. **568**, 130 (2018)
51. D. Li, Y. Liu, H. Liu, Z. Li, L. Lu, J. Liang, Z. Huang, W. Li, Res. Chem. Intermed. (2018)
52. H. Su, K.-X. Zhang, B. Zhang, H.-H. Wang, Q.-Y. Yu, X.-H. Li, M. Antonietti, J.-S. Chen, J. Am. Chem. Soc. **139**, 811 (2017)
53. S. Cheng, X. Meng, N. Shang, S. Gao, C. Feng, C. Wang, Z. Wang, New J. Chem. **42**, 1771 (2018)